



High-fidelity and long-distance entangled-state transfer with Floquet topological edge modesSenmao Tan,¹ Raditya Weda Bomantara ^{1,2,*} and Jiangbin Gong ^{1,†}¹*Department of Physics, National University of Singapore, Singapore 117543*²*Centre for Engineered Quantum Systems, School of Physics, University of Sydney, Sydney, New South Wales 2006, Australia*

(Received 15 September 2019; revised 2 May 2020; accepted 21 July 2020; published 10 August 2020)

We propose the generation of entangled qubits by utilizing the properties of edge states appearing at one end of a periodically driven (Floquet) superconducting qubit chain. Such qubits are naturally protected by the system's topology and their manipulation is possible through adiabatic control of the system parameters. By utilizing a Y-junction geometry, we then develop a protocol to perform high-fidelity transfer of entangled qubits from one end to another end of a qubit chain. Our quantum state transfer protocol is found to be robust against disorder and imperfection in the system parameters. More importantly, our proposed protocol also performs remarkably well at larger system sizes due to nonvanishing gaps between the involved edge states and the bulk states, thus allowing us in principle to transfer entangled states over an arbitrarily large distance. This work hence indicates that Floquet topological edge states are not only resourceful for implementing quantum gate operations, but also useful for high-fidelity and long-distance transfer of entangled states along solid-state qubit chains.

DOI: [10.1103/PhysRevA.102.022608](https://doi.org/10.1103/PhysRevA.102.022608)**I. INTRODUCTION**

Transferring quantum states from one place to another is an essential task in quantum information processing. The ubiquitous noise and device imperfections are, however, unavoidable and often limit the range for which a quantum state can be transferred with a good fidelity. Devising a scheme to effectively transfer quantum states over a long distance while minimizing the loss in fidelity has therefore been an active study since the last decade. Up to this date, various quantum state transfer (QST) protocols in many different platforms have been proposed, such as via strong coupling with photons [1–3] or coherent transfer along a chain of qubits [4–11]. In most cases, QST relies on the time evolution of a specifically designed Hamiltonian, and as such perfect QST may require a very precise control over some of the system parameters, which may pose some difficulties in its large-scale implementation. Reference [8] first proposed to use adiabatic control to facilitate robust quantum state transfer, but the dynamical phase induced by the adiabatic control field therein needs to be eliminated.

In a seemingly separate area, topological phases of matter have emerged as a new paradigm for designing novel devices that are naturally immune to local disorder or imperfection. For example, topological insulators and superconductors possess the so-called edge states at their boundaries whose properties are insensitive to the specific details of the system [12–15]. Such inherent robustness of edge states makes them ideal candidates for storing and processing quantum information. Indeed, the use of edge states for quantum computing has been extensively studied and has become an active

research area on its own [12,16–23]. In addition, the time evolution of symmetry-protected topological edge states often induces trivial dynamical phases (e.g., zero dynamical phase), a feature that can often simplify protocol designs for quantum information processing.

In recent years, several proposals to utilize edge states for QST have also emerged [24–27]. In Refs. [24,25], chiral edge states of a topological material are used to transfer quantum information stored in one qubit to another distant qubit. The ability to control the coupling between the input and output qubits with the edge states is thus necessary in such proposals, which may not be straightforward to implement and may induce additional errors. An alternative approach to harnessing topological phenomena for QST would be to design a transfer protocol which directly controls the system in which the qubits are encoded. This was explored in Refs. [26,27]. There, logical qubits are encoded at the edges of a superconducting qubit chain with dimerized coupling. By adiabatically tuning the qubit-qubit couplings in a prescribed manner, a logical qubit located at one end of the chain can be transferred to the other end [26,27]. Owing to the topological nature of the edge states, both logical qubit encoding and QST aspects of the protocol are inherently robust against common perturbations or disorder [26]. It is thus natural to generalize such a proposal for transferring entangled qubits from one end to the other. This possibility has also been explored in Ref. [26] by using trimerized instead of dimerized qubit-qubit couplings, although its implementation may be a challenge due to the extremely small energy gap in the protocol.

In this paper, we present another approach for transferring entangled qubits which are encoded in the edge states of a periodically driven (Floquet) topological system. Our study is further motivated by the capability of Floquet topological phases to exhibit features with no static analog, such as the existence of edge states pinned at quasienergy (the

*Raditya.Bomantara@sydney.edu.au

†phygj@nus.edu.sg

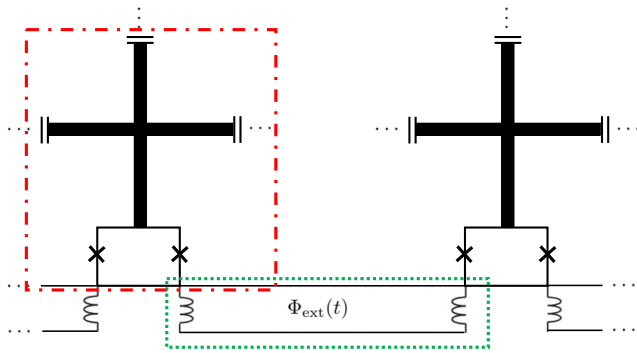


FIG. 1. A chain of Xmon qubits (red dash-dotted box) coupled to one another via tunable coupler (green dashed box). The external flux threading the tunable coupler realizes the time-periodic coupling between adjacent Xmon qubits.

analog of energy in Floquet systems) π/T [21,22,28–36] and anomalous edge states which do not satisfy the usual bulk-edge correspondence [37]. The former feature is particularly important in our present context, as the coexistence of the edge states pinned at both quasienergy zero and π/T naturally provides more channels for qubit encoding [21–23] and QST, as detailed below.

In the following, we describe our QST protocol based on a periodically driven Su-Schrieffer-Heeger model realized in a superconducting (Xmon) qubit chain [10,26]. It should be stressed, however, that our protocol can in principle also be implemented in a variety of other platforms capable of exhibiting one-dimensional topological phases, such as photonic wave-guide arrays [38,39] and acoustic systems [40]. The use of superconducting qubits to realize our QST protocol is, however, expected to be particularly promising for the following two reasons. First, the high tunability of the qubit-qubit coupling strength makes superconducting qubits an ideal platform to perform QST [10,41]. Second, with the current research trend of building quantum networks with superconducting qubits, it is an important task to achieve QST on such systems [10,26]. In particular, a type of superconducting qubit termed the Xmon qubit [42–45] offers further benefits in terms of high coherence time and fast coupling tunability [41–45]. Such an Xmon qubit comprises of a cross-shaped capacitor coupled to a superconducting quantum interference device (SQUID) (see the design inside the red box of Fig. 1). There, couplings between adjacent Xmon qubits are realized through the additional inductance elements connected to the qubits' SQUID components [42–45], whose strength is adjustable through the threading external flux (see the design inside the green box of Fig. 1). In such an Xmon qubit chain platform, the use of time-periodic coupling enables the existence of a pair of edge states at one end of the system, which we find to allow the creation of entangled qubits. An adiabatic manipulation protocol of the qubit-qubit couplings can then be devised to transfer such entangled qubits from one end to the other while maintaining a very good fidelity due to its topological protection. The main difference between our approach and that of Ref. [26] is twofold. First, entangled qubits can be prepared in a minimal setup with dimerized qubit-qubit couplings in our approach. Second, during the

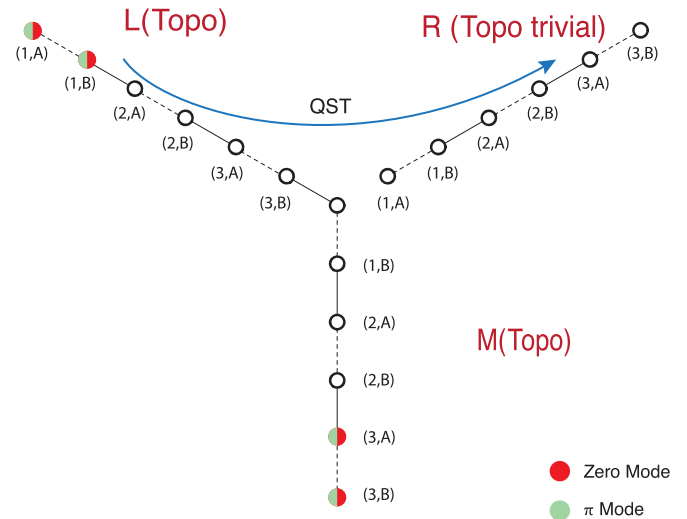


FIG. 2. A chain of superconducting qubits with dimerized couplings arranged in a Y-junction geometry. In a certain regime of system parameters, a pair of zero and π edge modes may emerge at one end of the L and M branches, which in the *ideal* case appear as antisymmetric and symmetric superpositions of the first (or the last) two qubits, respectively [see Eq. (8)].

adiabatic manipulation, the edge states remain pinned at quasienergy zero and π/T . As a result, large quasienergy gaps between the logical qubits and the rest of the qubits are maintained throughout the protocol, which is necessary for adiabaticity to hold. Our proposal thus demonstrates that while Floquet topological phases enable more qubits to be encoded as compared with their static counterpart under the same physical constraints, such qubits can also be transferred from one place to another using an approach similar to that in typical static systems.

This paper is structured as follows. In Sec. II, we introduce the model studied in this paper, briefly review the emergence of zero and π modes in the model and the topological invariants that characterize them, and set up some notation. In Sec. III, we propose a protocol to generate entangled qubits from the ground states of the underlying static model by utilizing the properties of the zero and π modes that exist after the periodic driving is turned on. In Sec. IV, we present a protocol to transfer an entangled qubit from one end to another along a Y-shaped chain of periodically driven Xmon qubits. In Sec. V, we verify the robustness of our QST protocol in the presence of disorder and imperfection; then we also show how our proposal can be adapted to improve the previous QST protocol in Ref. [26], enabling high-fidelity QST even for long qubit chains. Finally, we conclude our paper and present potential future directions in Sec. VI.

II. MODEL AND QUBIT ENCODING

We consider a chain of superconducting qubits arranged in a Y-junction geometry with dimerized nearest-neighbor time-periodic couplings, as depicted in Fig. 2. Each circle represents a superconducting Xmon qubit and is categorized into sublattice A or B based on how it couples with its two neighboring qubits. The dashed and solid lines mark two

different coupling strengths between two such qubits, which are referred to as intra- and interlattice coupling, respectively. L, R, and M label the three branches of the system, each of which is described by a Hamiltonian of the following form:

$$H^{(c)}(t) = \begin{cases} H_1^{(c)}(t) & \text{for } (m-1)T < t < (m-1/2)T \\ H_2^{(c)}(t) & \text{for } (m-1/2)T < t < mT, \end{cases}$$

$$H_1^{(c)}(t) = \sum_j (-J_{\text{intra},j}^c \sigma_{B,j}^{c\dagger} \sigma_{A,j}^c + \text{H.c.}), \quad (1)$$

$$H_2^{(c)}(t) = \sum_j (-j_{\text{inter},j}^c \sigma_{B,j}^{c\dagger} \sigma_{A,j+1}^c + \text{H.c.}), \quad (2)$$

where $c \in \{L, R, M\}$ labels one of the three branches, A and B are the indices of the sublattice site, $\sigma_{S,j}^\dagger = |e\rangle\langle g|_{S,j}$ is the qubit raising operator at sublattice S of unit cell j , $|g\rangle_j$ and $|e\rangle_j$ are the ground and excited states of the j th Xmon qubit, J_{intra} is the intralattice coupling strength in H_1 and j_{inter} is the interlattice coupling strength in H_2 . To simplify our analysis, we only consider the intralattice coupling in the first half of the period and the interlattice coupling in the second half. Unless otherwise specified, we take $J_{\text{intra},j}^c = J_1^c$ and $j_{\text{inter},j}^c = j_2^c$ in the following.

The spectral properties of such a time-periodic system are characterized by quasienergies, defined as the eigenphase of the one-period propagator (Floquet operator [46,47]),

$$U|\epsilon\rangle = \exp(-i\epsilon T)|\epsilon\rangle, \\ U \equiv \mathcal{T} \exp\left(\int_{t_0}^{t_0+T} -\frac{iH(t)}{\hbar} dt\right), \quad (3)$$

where \mathcal{T} is the time-ordering operator, ϵ is the quasienergy, and $|\epsilon\rangle$ is the Floquet eigenstate with quasienergy ϵ . By construction, ϵ is only defined modulo $\frac{2\pi}{T}$. As such, edge states may form not only in the gap around quasienergy zero, which are commonly found in static systems, but also in the gap around quasienergy π/T .

In the momentum space, the two Hamiltonians defined in Eq. (2) take the form

$$\mathcal{H}_\alpha^{(c)}(k, t) = -(h_{a,\alpha}^{(c)} + h_{b,\alpha}^{(c)} \cos(k))\tau_x + h_{b,\alpha}^{(c)} \sin(k)\tau_y, \quad (4)$$

where $\alpha = 1, 2$, τ 's are Pauli matrices acting in the sublattice space, $h_{a,1}^{(c)} = J_1^c$, $h_{b,1}^{(c)} = 0$, and $h_{b,2}^{(c)} = j_2^c$, $h_{a,2}^{(c)} = 0$. By taking $t_0 = T/4$ in Eq. (3), the momentum space Floquet operator can be written as (we take $\hbar = \frac{T}{2} = 1$ from here onwards)

$$U_{\text{sym}}(k) = F(k)G(k), \\ F(k) = \exp(-iH_2(k)/2) \exp(-iH_1(k)/2), \\ G(k) = \exp(-iH_1(k)/2) \exp(-iH_2(k)/2). \quad (5)$$

It follows that $U_{\text{sym}}(k)$ possesses a chiral symmetry defined by the operator $\Gamma = \tau_z$, such that $\Gamma U_{\text{sym}}(k) \Gamma^\dagger = U_{\text{sym}}(k)^\dagger$. As a result, its edge states under open boundary conditions are pinned at exactly zero and/or π/T quasienergies (termed zero and π modes, respectively), whose numbers are determined by the topological invariants defined in Refs. [28,29]. In particular, since $F(k) = \Gamma^\dagger G(k)^\dagger \Gamma$, such invariants can be obtained from $F(k)$ only. That is, by writing the 2×2 matrix

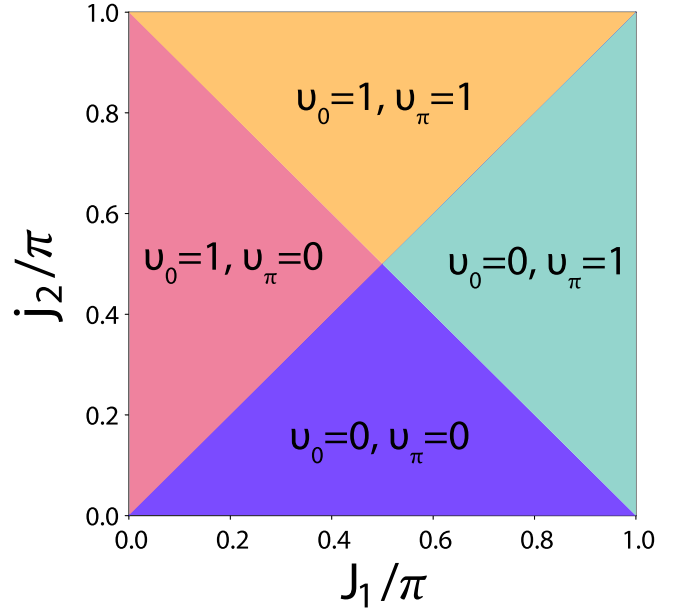


FIG. 3. The phase diagram of the topological invariants ν_0 and ν_π as a function of J_1 and j_2 .

representation of F in the canonical ($\Gamma = \tau_z$) basis as

$$F(k) = \begin{pmatrix} a(k) & b(k) \\ c(k) & d(k) \end{pmatrix}, \quad (6)$$

the topological invariants counting the number of zero and π modes are respectively given by [28,29]

$$\nu_0 = \frac{1}{2\pi i} \int_{-\pi}^{\pi} dk \left(b^{-1} \frac{d}{dk} b \right), \quad (7)$$

$$\nu_\pi = \frac{1}{2\pi i} \int_{-\pi}^{\pi} dk \left(d^{-1} \frac{d}{dk} d \right). \quad (8)$$

In Fig. 3, we numerically compute ν_0 and ν_π under some representative parameter values, which we have also analytically verified in Appendix A.

In the following, we are mostly interested in the yellow and purple regime of Fig. 3, corresponding to the presence and absence of both zero and π modes, respectively. In particular, we initialize our system such that branches L and M are in the yellow regime, whereas branch R is in the purple regime. For analytical solvability, we further consider the following parameter values (referred to as the ideal case) for the yellow regime, $J_1^{L,M} = i\pi/2$, $j_2^{L,M} = i\pi$, and for the purple regime, $J_1^R = i\pi/2$, $j_2^R = 0$, in the presentation of our state preparation and QST protocols, where such imaginary couplings are indeed realizable in superconducting qubit setups [10]. We show, however, through some numerical calculations, that such fine tuning is not necessary in the actual implementation of our protocols.

In the ideal case, one pair of zero and π modes is localized at the first two qubits (the first unit cell) of the L branch. By further taking $t_0 = 0$ in Eq. (3), the zero and π modes localized near the left end can be explicitly obtained as [48]

$$|0\rangle^{(L)} = (|eg\rangle_1^{(L)} - |ge\rangle_1^{(L)}) \otimes G', \\ |\pi\rangle^{(L)} = (|eg\rangle_1^{(L)} + |ge\rangle_1^{(L)}) \otimes G', \quad (9)$$

where subscript is the site index and $G' = \prod_{i \neq 1} |gg\rangle_i$ denotes the ground state of the other Xmon qubits in the system, which are suppressed in the rest of this paper. In particular, we assume that quantum information is initially encoded in the first two Xmon qubits of the L branch, i.e., the subspace spanned by $\{|gg\rangle_1^{(L)}, |ge\rangle_1^{(L)}, |eg\rangle_1^{(L)}, |ee\rangle_1^{(L)}\}$, which is then transferred to the last two Xmon qubits of the R branch, i.e., the subspace spanned by $\{|gg\rangle_N^{(R)}, |ge\rangle_N^{(R)}, |eg\rangle_N^{(R)}, |ee\rangle_N^{(R)}\}$ (N being the size of the R branch), through appropriate adiabatic deformation of some system parameters. In this case, we note that the zero and π edge modes defined above then represent two maximally entangled states between two qubits, and the carefully designed adiabatic deformation leads to the movement of the domain wall accommodating these edge modes from one end of the L branch to the other end of the R branch, so that the L (R) branch becomes a topologically trivial (nontrivial) regime at the end of the transfer protocol. In particular, the former also implies that the task of preparing an entangled state then reduces to the task of preparing a Floquet edge state, the latter of which can be accomplished via a protocol introduced in the next section. Finally, since zero and π modes must appear in pairs at two opposite edges, another set of zero and π modes exists at the end of the M branch. These zero and π modes will remain there at all times, and by taking the size of the M branch to be sufficiently large, quantum information leakage due to hybridization between pairs of zero and π modes during the QST process can be avoided.

III. ENTANGLED QUBITS GENERATION

Suppose that our system starts in a ground state of a static Hamiltonian $H = H_2^{(L)} + H_2^{(M)} + H_2^{(R)}$, before we switch on the periodic driving at some time t_0 . Without loss of generality, we may assume that this corresponds to the initial state of $|\psi_0\rangle = |eg\rangle_1^{(L)} \propto |0\rangle^{(L)} + |\pi\rangle^{(L)}$, which is thus a simple product state. Our objective in this section is to devise a protocol based on a series of adiabatic variations of some qubit-qubit couplings in the system, such that the above initial state evolves to either $|0\rangle^{(L)}$ or $|\pi\rangle^{(L)}$ at the end of the protocol. This can be accomplished by adapting the protocol introduced by two of us in Ref. [21] which amounts to transforming zero and π modes as $|0\rangle^{(L)} \rightarrow (|0\rangle^{(L)} - |\pi\rangle^{(L)})/\sqrt{2}$ and $|\pi\rangle^{(L)} \rightarrow (|0\rangle^{(L)} + |\pi\rangle^{(L)})/\sqrt{2}$. To this end, it suffices to restrict our attention to branch L, so that we remove the (L) index in the following. We now present our protocol in three steps, which is also summarized in Fig. 4.

In step 1, we adiabatically deform the Hamiltonian stroboscopically (by slowly varying it at every period) to move the zero and π modes from the first to the third unit cell in the L branch. This is accomplished by setting $j_{\text{inter},2} = j_2 \cos \phi$ and at the same time introducing a new coupling $h_2^{(1)} = j_2 \sin \phi \sigma_{A,1}^\dagger \sigma_{B,2} + \text{H.c.}$ into H_2 , where ϕ is the adiabatic parameter which is swept from zero to $\pi/2$. It can be shown that the zero and π modes at any stroboscopic time take the form [21]

$$|0\rangle = \cos \phi (|eg\rangle_1 - |ge\rangle_1) - \sin \phi (|eg\rangle_3 - |ge\rangle_3), \quad (10)$$

$$|\pi\rangle = \cos \phi (|eg\rangle_1 + |ge\rangle_1) - \sin \phi (|eg\rangle_3 + |ge\rangle_3). \quad (11)$$

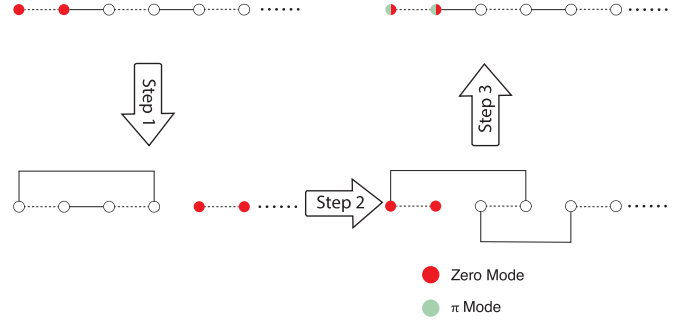


FIG. 4. Schematic of the adiabatic protocol resulting in a $\pi/4$ rotation in the subspace spanned by the zero and π modes. Here we focus on the L branch and highlight only the evolution of the zero mode (red solid circles), which at the end transforms into a superposition of zero and π modes (red and green half-filled circles). Dashed (solid) lines represent the qubit-qubit coupling appearing in H_1 (H_2).

At the end of this step, $|0\rangle$ adiabatically changes from $(|eg\rangle_1 - |ge\rangle_1)$ to $(-|eg\rangle_3 + |ge\rangle_3)$, whereas $|\pi\rangle$ transforms from $(|eg\rangle_1 + |ge\rangle_1)$ to $(-|eg\rangle_3 + |ge\rangle_3)$; i.e., both zero and π modes are now shifted to the third unit cell as intended.

In step 2, starting from the end of step 1, we continue to adiabatically deform the system's Hamiltonian by taking $j_{\text{inter},1} = j_2 \cos \phi$ and introducing a new term $h_2^{(2)} = j_2 \sin \phi \sigma_{A,2}^\dagger \sigma_{A,3} + \text{H.c.}$ into H_2 , where ϕ again changes slowly every period from zero to $\pi/2$ at the end of this step. We can again show that at any stroboscopic time [21]

$$|0\rangle = -\sin \phi (|eg\rangle_1 + |ge\rangle_1) + \cos \phi (-|eg\rangle_3 + |ge\rangle_3), \quad (12)$$

$$|\pi\rangle = \sin \phi (-|eg\rangle_1 + |ge\rangle_1) - \cos \phi (|eg\rangle_3 + |ge\rangle_3). \quad (13)$$

That is, $|0\rangle$ transforms to $-|eg\rangle_1 - |ge\rangle_1$, whereas $|\pi\rangle$ transforms to $(-|eg\rangle_1 + |ge\rangle_1)$ at the end of this step.

In step 3, we recover the system's original Hamiltonian by returning $j_{\text{inter},1}$ and $j_{\text{inter},2}$ back to their original values as $j_{\text{inter},1} = j_{\text{inter},2} = j_2 \cos \phi$ and slowly decreasing $h_2^{(1)}$ and $h_2^{(2)}$ to zero as $h_2^{(1)} \rightarrow h_2^{(1)} \cos^2 \phi$ and $h_2^{(2)} \rightarrow h_2^{(2)} \cos^2 \phi$ with ϕ being slowly swept from zero to $\pi/2$. However, in order to induce a nontrivial rotation in the subspace spanned by zero and π modes, we only tune the adiabatic parameter ϕ every other period. As demonstrated in Ref. [21], this leads to the transformation $|0\rangle \rightarrow (|0\rangle - |\pi\rangle)/\sqrt{2}$ and $|\pi\rangle \rightarrow (|0\rangle + |\pi\rangle)/\sqrt{2}$ at the end of this step, thus completing our protocol.

To explicitly demonstrate how an entangled state can be generated via the protocol above, in Fig. 5 we numerically plot the overlap between the state $|\psi(t)\rangle$, initially prepared in the product state $|eg\rangle_1$, and the zero (π) mode of the original system, both of which represent a maximally entangled two qubit states [see Eq. (9)]. In particular, since its overlap with the zero mode becomes unity at the end of the adiabatic protocol, our state transforms into $|0\rangle = |eg\rangle_1 - |ge\rangle_1$. In practice, for superconducting Xmon qubits with $j_2/2\pi = 50$ MHz, the qubit generation process in Fig. 5 takes 6 μs , which is far less than the energy relaxation time of Xmon qubits (approximately 50 μs) [10,41]. To generate another entangled state $|\pi\rangle = |eg\rangle_1 + |ge\rangle_1$, we can simply perform exactly the same protocol two more times. That is, starting with $|eg\rangle_1^{(L)}$, the

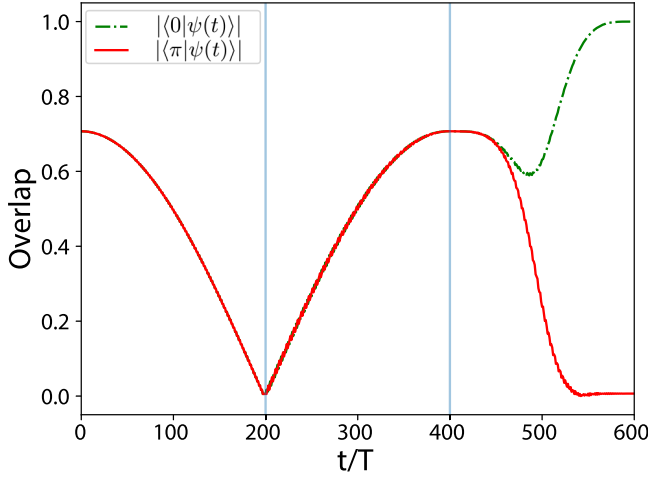


FIG. 5. Time evolution of the overlap $|\langle 0|\psi(t)\rangle|$ and $|\langle \pi|\psi(t)\rangle|$ for a state initially prepared as a superposition of zero mode and π mode, i.e., $|\psi(0)\rangle = \frac{1}{\sqrt{2}}(|0\rangle + |\pi\rangle)$. Each step takes 200 periods to complete.

application of the above protocol once, twice, and three times yields $|0\rangle = |eg\rangle_1 - |ge\rangle_1$, $|0\rangle = |ge\rangle_1$, $|0\rangle = |\pi\rangle = -|ge\rangle_1$, and $|\pi\rangle = -|eg\rangle_1 - |ge\rangle_1$, respectively.

In principle, we can also prepare a more generic entangled state by exploiting the dynamical evolution of the Floquet operator within a driving period. In particular, since $|0\rangle$ and $|\pi\rangle$ pick up different dynamical phases during their time evolution, evolving a state initially prepared in either $|0\rangle$ or $|\pi\rangle$ to a specific time $t^* < T$ can in principle lead to a desired arbitrary entangled state $|\psi\rangle = \alpha|eg\rangle_1 + \beta|ge\rangle_1$ (see Appendix C for an explicit example). In general, however, this mechanism will lead to a lower fidelity as compared with that based on the protocol described above, and as such a distillation protocol might also need to be supplemented in the actual implementation of such an arbitrary entangled state generation.

IV. QUANTUM STATE TRANSFER

In the previous section, we have shown how entangled qubits arise as either a zero or π mode. In general, a generic entangled qubit can be encoded as a superposition of zero and π modes, $|\psi\rangle = \alpha|eg\rangle_1 + \beta|ge\rangle_1 = \frac{\alpha+\beta}{2}|0\rangle + \frac{\alpha-\beta}{2}|\pi\rangle$. In this section, we propose a protocol to transfer these zero and π modes (and thus any entangled qubits) from the leftmost end (L branch) to the rightmost end (R branch) of the chain. To this end, the importance of using Y-junction geometry to facilitate such a QST is now clear. That is, in a strictly one-dimensional chain of such Xmon qubits, both zero and π modes necessarily emerge at both ends. As a result, transferring a zero or π mode from one end to the other necessarily leads to the interference with zero or π mode located at the other end, thus destroying the transferred information. By utilizing a Y-junction geometry, we can instead adjust our system such that one pair of zero and π modes is located at the end of the L branch, whereas the other is at the end of the M branch. By encoding our information in the zero and π modes originally located in the L branch, we can

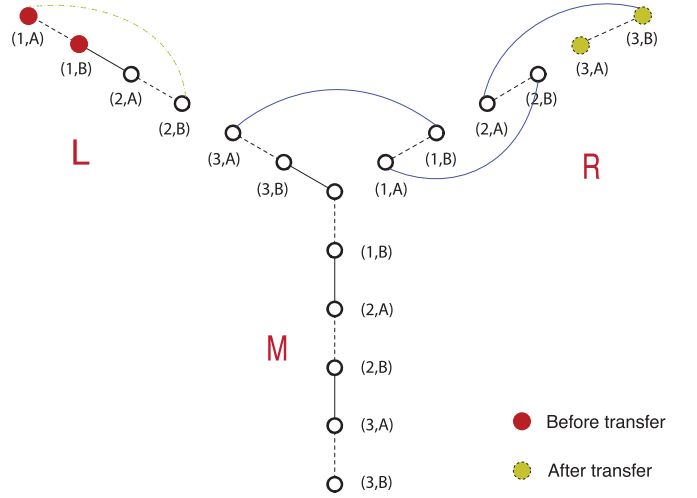


FIG. 6. Schematic diagram of the QST protocol. The green dash-dotted line represents the coupling added in phase I of QST and the blue line represents the coupling added in phase II. Again, dashed lines represent the coupling in H_1 and solid lines present the coupling in H_2 .

faithfully transfer such information to the other end of the R branch, thus completing our QST procedure. Such a transfer can then be accomplished by performing a series of adiabatic manipulations, which can be divided into two phases below and summarized in Fig. 6.

Phase I. Transfer zero and π modes from the end of the L branch to the middle point in $(N_L - 2)/4$ steps, N_L being the number of qubits in the L branch. In the x th step, a new term is introduced in H_2 , i.e., $h_x^{(3)} = j_2 \sin \phi_x \sigma_{A,2x-1}^{(L)\dagger} \sigma_{B,2x}^{(L)} + \text{H.c.}$, and we set the coupling strength $j_{\text{inter},2x} = j_2 \cos \phi_x$, where ϕ_x is the parameter adiabatically increasing from 0 to $\pi/2$. As detailed in Appendix B 1, the zero and π modes at any stroboscopic time within the x th step are found as

$$|0\rangle^{(L)} = \frac{1}{\sqrt{2}} [\cos \phi_x (|eg\rangle_{2x-1}^{(L)} - |ge\rangle_{2x-1}^{(L)}) + \sin \phi_x (|eg\rangle_{2x+1}^{(L)} - |ge\rangle_{2x+1}^{(L)})], \quad (14)$$

$$|\pi\rangle^{(L)} = \frac{1}{\sqrt{2}} [\cos \phi_x (|eg\rangle_{2x-1}^{(L)} + |ge\rangle_{2x-1}^{(L)}) + \sin \phi_x (|eg\rangle_{2x+1}^{(L)} + |ge\rangle_{2x+1}^{(L)})]. \quad (15)$$

At the end of this phase, i.e., after completing the $[(N_L - 2)/4]$ th step, both zero and π modes are transferred to the middle point of the Y junction; i.e.,

$$|0\rangle^{(L)} : |eg\rangle_1^{(L)} - |ge\rangle_1^{(L)} \rightarrow |eg\rangle_{N_L}^{(L)} - |ge\rangle_{N_L}^{(L)}, \quad (16)$$

$$|\pi\rangle^{(L)} : |eg\rangle_1^{(L)} + |ge\rangle_1^{(L)} \rightarrow |eg\rangle_{N_L}^{(L)} + |ge\rangle_{N_L}^{(L)}. \quad (17)$$

Phase II. Transfer zero and π modes from the middle point to the end of the R branch in $N_R/2$ steps, N_R being the number of qubits in the R branch. In the x th step, a new term, $h_x^{(4)} = j_2 \sin \phi_x \sigma_{A,x-1}^{(R)\dagger} \sigma_{B,x}^{(R)} + \text{H.c.}$, is introduced in H_2 , where ϕ_x is the adiabatic parameter swept slowly at every period from zero to $\pi/2$, and $\sigma_{A,0}^{(R)} \equiv \sigma_{A,N_L}^{(L)}$. As detailed in

Appendix B 2, the zero and π modes at any stroboscopic time within the x th step are

$$|0\rangle^{(L)} = \frac{1}{\sqrt{2}} \left[\cos\left(\frac{\pi}{2} \sin \phi_x\right) (|eg\rangle_x^{(R)} - |ge\rangle_x^{(R)}) + \sin\left(\frac{\pi}{2} \sin \phi_x\right) (-|eg\rangle_{x+1}^{(R)} + |ge\rangle_{x+1}^{(R)}) \right], \quad (18)$$

$$|\pi\rangle^{(L)} = \frac{1}{\sqrt{2}} \left[\cos\left(\frac{\pi}{2} \sin \phi_x\right) (|eg\rangle_x^{(R)} + |ge\rangle_x^{(R)}) + \sin\left(\frac{\pi}{2} \sin \phi_x\right) (|eg\rangle_{x+1}^{(R)} + |ge\rangle_{x+1}^{(R)}) \right]. \quad (19)$$

At the end of this phase, i.e., after completing the $(N_R/2)$ th step, the zero and π modes are perfectly transferred to the right end of branch R:

$$|0\rangle^{(L)} : (-1)^{N_R/2} (|eg\rangle_{N_R}^{(R)} - |ge\rangle_{N_R}^{(R)}), \quad (20)$$

$$|\pi\rangle^{(L)} : |eg\rangle_{N_R}^{(R)} + |ge\rangle_{N_R}^{(R)}. \quad (21)$$

In this case, it is also worth noting that the L branch now becomes topologically trivial, whereas the R branch is in the topologically nontrivial regime.

To perform a long-distance QST over 40 qubits with configuration $N_L = 22$, $N_R = 18$, and $N_M = 8$, where each step takes 70 periods to complete, for superconducting Xmon qubits with maximal coupling strength $j_2/2\pi = 50$ MHz, the QST completes in 19 μ s, which is within the coherence time of Xmon qubits (approximately 50 μ s) [10,41]. While the above protocol is presented in the *ideal* case, i.e., based on special parameter values discussed in Sec. II, the actual implementation of our protocol does not rely on such fine tuning. Indeed, as long as the zero and π modes in the system remain well separated in quasienergies from the bulk states during the adiabatic manipulations [see, e.g., Fig. 7(a)], the above QST protocol is still expected to work with a good fidelity (this aspect is further discussed in the next section). Moreover, the fact that zero and π modes remain at quasienergy zero and π/T , respectively, at all times means that chiral symmetry is respected throughout the whole protocol, thus implying the topological robustness of the QST process. This aspect is especially expected since, as illustrated in Fig. 6, our QST protocol involves only couplings between sublattice A and B, corresponding to terms proportional to τ_x and τ_y , which are thus compatible with the chiral operator τ_z associated with the system's instantaneous Hamiltonian. Finally, it is worth commenting on the possible existence of chiral-symmetry-breaking terms, which may be detrimental for the implementation of our protocol, in actual experiments. Within the framework of the Xmon qubit chain where the current proposal is envisioned, we note that such terms may potentially arise if the different Xmon qubits in the chain have considerably different transition frequencies. However, given that current state-of-the-art experiments involving Xmon qubits [44,45] suggest the possibility to control qubits' frequencies to a very high precision, we expect that such chiral-symmetry-breaking terms can in principle be avoided.

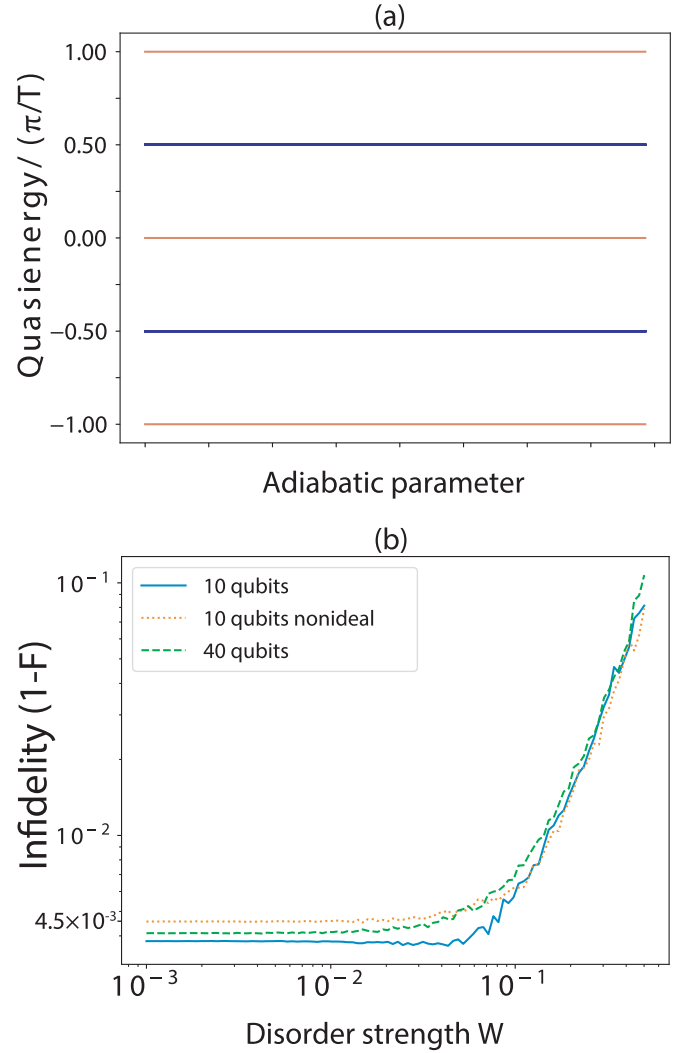


FIG. 7. (a) The quasienergy spectrum of our system during QST. Notice that quasienergies zero and π/T , which correspond to our zero and π modes, respectively, remain well separated from the other quasienergies at all times. (b) Infidelity ($1 - |\langle \psi_f | \psi_d \rangle|$) against the disorder strength. In the 10-qubit system, we take $N_L = 6$, $N_R = 4$, and $N_M = 8$, whereas in the 40-qubit system, we take $N_L = 22$, $N_R = 18$, and $N_M = 8$. The parameters used for the nonideal case (the orange dotted line) are $J_1 = 1.5i$, $j_2^i = j_2^M = 3i$, $j_2^R = -0.1i$, and $J_2 = j_1 = 0$. Each step takes 39 (70) periods to complete in the 10-qubit (40-qubit) system and each data point is averaged over 100 disorder realizations.

V. DISCUSSION

In practice, perfect modulation of the coupling strengths is impossible. As such, we now examine the robustness of the QST protocol presented in Sec. IV against coupling disorders, which are implemented by adding each of the following terms to H_1 and H_2 , respectively:

$$\Delta H_1 = \sum_{c \in C} \sum_m (\delta_{1,m} J_1 \sigma_{B,m}^{c\dagger} \sigma_{A,m}^c + \text{H.c.}),$$

$$\Delta H_2 = \left[\sum_{c \in \{L,M\}} \sum_m (\delta_{2,m} J_2 \sigma_{B,m}^{c\dagger} \sigma_{A,m+1}^c + \text{H.c.}) \right]$$

$$\begin{aligned}
& + \sum_{m'} (\delta_{3,m'} j_2 \sigma_{A,2m'-1}^{L\dagger} \sigma_{B,2m'}^L + \text{H.c.}) \\
& + \sum_{m''} (\delta_{4,m''} j_2 \sigma_{A,m''-1}^{R\dagger} \sigma_{B,m''}^R + \text{H.c.}) \Big], \quad (22)
\end{aligned}$$

where $\delta_{i,m}$ is a uniform random number taken $\in [-0.5W, 0.5W]$ and W is the disorder strength. In addition to disorders introduced in the original system, we further consider the presence of disorders during the numerical implementation of the QST protocol introduced in Sec. IV. This is accomplished by modifying the newly added couplings $h_x^{(3)} = \sin \phi_x j_2 (1 + \delta_x^{(3)}) \sigma_{A,2x-1}^{(R)\dagger} \sigma_{B,2x}^{(R)} + \text{H.c.}$ and $h_x^{(4)} = \sin \phi_x j_2 (1 + \delta_x^{(4)}) \sigma_{A,2x-2}^{(R)\dagger} \sigma_{B,2x-1}^{(R)} + \text{H.c.}$

By denoting the transferred state as $|\psi_i\rangle$ in the ideal case and $|\psi_d\rangle$ in the case with disorders, we numerically calculate the infidelity $1 - F = 1 - |\langle \psi_i | \psi_d \rangle|$ as a function of the disorder strength in Fig. 7(b). In addition to the robustness of our QST protocol against small to moderate disorders, the orange line of Fig. 7(b) also demonstrates the good performance of our QST protocol at other system parameters, such as $J_1 = 1.5i$, $j_2^L = j_2^R = 3i$, $j_2^R = -0.1i$, and $J_2 = j_1 = 0$, which deviate rather significantly from the ideal case in which our QST protocol is analytically solvable.

We also note that phase I and phase II of our QST protocol can in principle be sped up by performing the actions in all $(N_L - 2)/4$ and $N_R/2$ steps in one go. That is, starting with $|0\rangle^{(L)}$ and $|\pi\rangle^{(L)}$ localized at the left end of the L branch, one can introduce $h^{(3)} = \sum_x h_x^{(3)}$ and $h^{(4)} = \sum_x h_x^{(4)}$ in H_2 and take $j_{\text{inter},2} = j_{\text{inter},4} = \dots = j_{\text{inter},N_L-1} = j_2 \cos \phi$ simultaneously to move $|0\rangle^{(L)}$ and $|\pi\rangle^{(L)}$ to the right end of the R branch. While this approach works very well for sufficiently small systems, increasing the number of qubits will inevitably cause the transferred state to become more delocalized in the middle of such a direct-transfer protocol, leading to the unavoidable closing of the quasienergy spectrum as shown in Fig. 8(b). By contrast, the step-by-step QST protocol introduced in Sec. IV ensures that the transferred state remains localized at all times, thus maintaining large quasienergy gaps between zero or π modes and the bulk quasienergies, even for a very large number of qubits. In such cases, the step-by-step protocol is expected to perform better as compared with the direct-transfer protocol, which we have also verified in Fig. 8(a) for the case of 68 qubits.

Inspired from the above analysis, we may also propose an improvement to the QST protocol introduced in Ref. [26]. In particular, Ref. [26] proposes a similar QST protocol by using a chain of Xmon qubits with time-dependent coupling. Due to the lack of π modes in static systems, however, the use of dimerized coupling in such a chain only enables the transfer of a single qubit from one end to the other, which Ref. [26] proposed to accomplish in one step by simultaneously modulating all the qubit-qubit couplings. While their results show a good QST fidelity for a small number of qubits, the same problem of the vanishing energy gap will also arise for a larger number of qubits. As such, the idea of breaking down the QST process into steps in the spirit of our protocol in Sec. IV can also be adapted to enable high-fidelity transfer of one qubit in such a static system scenario. To this end, we recall the static Hamiltonian used in Ref. [26] describing the dimerized

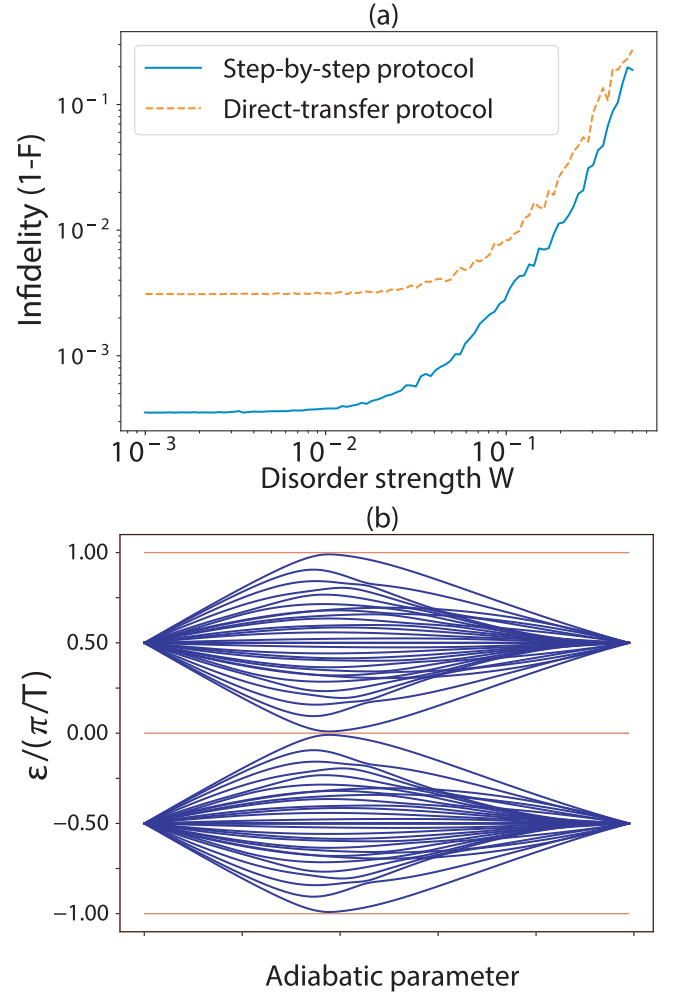


FIG. 8. (a) Comparison of the infidelity against disorder strength between our proposed step-by-step protocol in Sec. IV and the direct-transfer protocol. Both systems have the size $N_L = 30$, $N_R = 30$, ad $N_M = 8$ and the total time for both QSTs is 6600 periods. (b) Quasienergy spectrum of the direct-transfer protocol during the QST process. Notice that the quasienergy gap vanishes somewhere during the process, leading to the corruption of the transferred information and thus lower fidelity. The quasienergy spectrum of the step-by-step protocol can be seen in Fig. 7(a).

qubit-qubit couplings in a chain of Xmon qubits,

$$\hat{H} = \sum_{j=1}^N (J_0^j \hat{\sigma}_{A,j}^\dagger \hat{\sigma}_{B,j} + J_1^j \hat{\sigma}_{B,j}^\dagger \hat{\sigma}_{A,j+1} + \text{H.c.}). \quad (23)$$

In Ref. [26], QST is accomplished by adiabatically tuning all J_1^j and J_0^j simultaneously as $J_i^j = g(1 + (-1)^i \cos \theta)$, with θ being the adiabatic parameter swept from zero to π . In our proposed improvement, we may instead break down the QST protocol into $N - 1$ steps. In the x th step, we take $J_i^x = g(1 + (-1)^i \cos \theta_x)$ while keeping the other coupling strengths constant, with θ_x being the same adiabatic parameter swept from zero to π . This amounts to transferring a qubit from the x th unit cell to the $(x + 1)$ th unit cell, so that after the $(N - 1)$ th step, the qubit originally at the left end of the lattice is perfectly transferred to the right end. In this improved

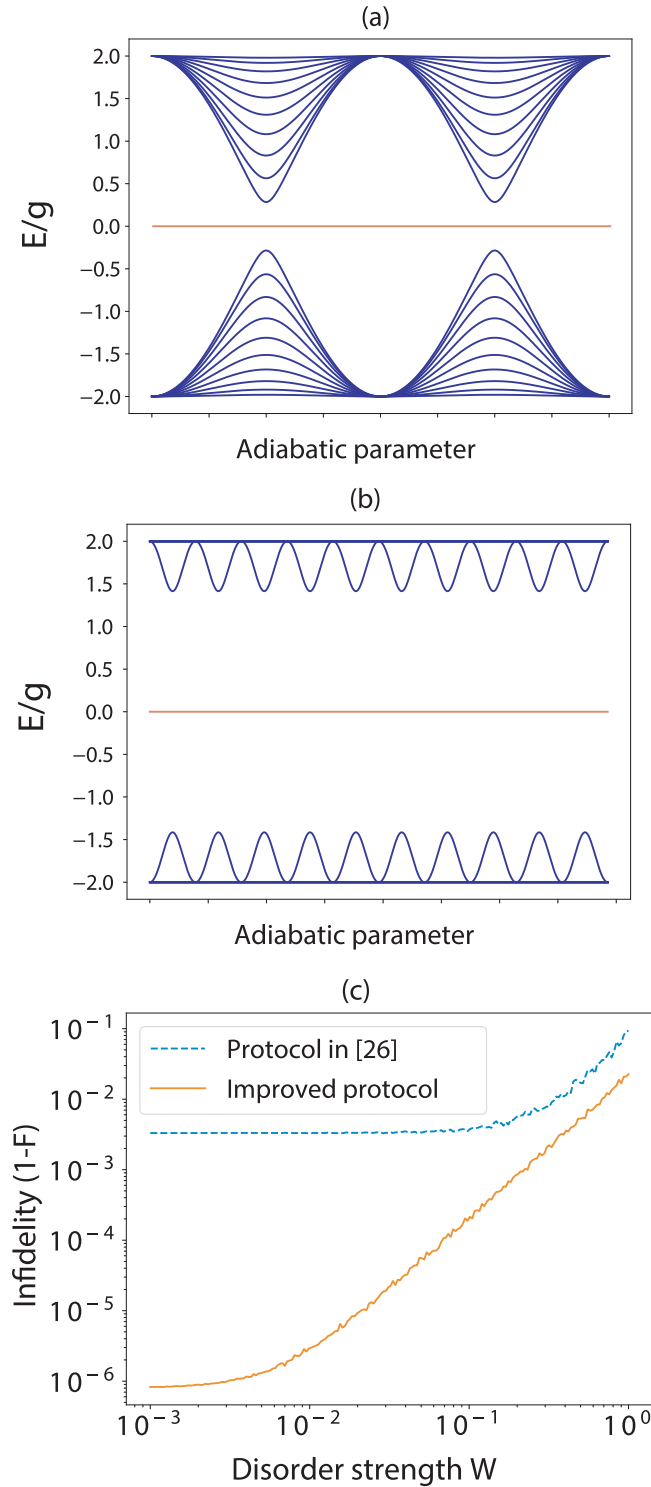


FIG. 9. (a) The energy band spectrum of a single qubit transfer along a chain of 21 Xmon qubits of Ref. [26] by performing the transfer in one go. (b) Same as in (a), but we divide the QST process into 20 steps. (c) Comparison of the infidelity as a function of the disorder strength between the two protocols in (a) and (b). The total adiabatic time for both QST protocols is $t_{\text{tot}} = \pi/(0.01g)$.

QST protocol, the gap in the energy spectrum is significantly larger than the original protocol, as illustrated in Figs. 9(a) and 9(b). To further test the robustness of this improved protocol, we again consider the presence of disorders by adding the

following term to the original Hamiltonian of Eq. (23):

$$\hat{H}_d = \sum_j (J_0^j \delta_{0,j} \hat{\sigma}_{A,j}^\dagger \hat{\sigma}_{B,j} + J_1^j \delta_{1,j} \hat{\sigma}_{B,j}^\dagger \hat{\sigma}_{A,j+1} + \text{H.c.}), \quad (24)$$

where $\delta_{0,j}$ and $\delta_{1,j}$ are random numbers taken $\in [-0.5W, 0.5W]$ and W is the disorder strength. The infidelity as a function of the disorder strength is plotted in Fig. 9(c). To have a fair comparison, the total transfer time is the same for the two protocols, $t_{\text{tot}} = \pi/(0.01g)$. It is clear that our proposed protocol indeed improves the robustness of such a system during QST. To conclude, breaking down the QST process into steps is one of our main results in this paper, which can be applied to improve the fidelity of adiabatic-based QST for large system sizes, both in time-periodic and static settings. This in turn enables us, at least in principle, to transfer qubits over an arbitrarily large distance.

Finally, despite the advantages of employing the time-periodic system highlighted in this paper, we should also comment on two potential challenges in its implementation. First, while we have demonstrated the robustness of our protocol against spatial disorders, it can be more vulnerable to temporal disorders (see Appendix D for the explicit analysis regarding the performance of our QST protocol under temporal disorders). This is, however, a typical issue commonly found in Floquet systems and, as such, efforts have been made in recent years to study and mitigate the effect of such temporal disorders [49]. On the other hand, with current technologies, we expect that the implementation of sufficiently precise periodicity may not actually be impossible in the actual experimental implementations, given that indeed experimental observations of Floquet phases have been made over the years [50,51]. Combined with the existence of a near-perfect plateau at small enough temporal noise depicted in Appendix D, there is therefore hope to verify our presented protocol in experiments in the near future.

A second potential problem expected in Floquet systems is thermalization due to interaction (where an exception to this is expected for a class of Floquet systems with many-body localizations (MBLs) [52–55] or coupled to a cold reservoir [56]). In the model system considered here, the quantum information transfer always, as indicated by our model itself, occurs within the single-qubit excitation subspace (so many-body interaction is not there in the ideal case). In the physical platform here, error on the hardware level more likely causes population leakage from the Hilbert space under consideration, rather than interaction effects as in a many-electron system. Furthermore, suppose there are weak many-body interactions resulting from certain unknown error and hence thermalization becomes unavoidable; it may in practice take place at a timescale longer than that which is typically relevant in experiments. For instance, while MBL is considered necessary for the formation of a recently discovered Floquet phase termed the Floquet time crystal [57], an experiment done in Ref. [50] demonstrates the observation of some Floquet time crystal signatures, at least within the timescale considered therein. Therefore, it is still possible to avoid the seemingly detrimental effect of thermalization even in the presence of many-body interactions. Overall, the interaction effects in Floquet topological phases in general are still an open problem.

VI. CONCLUDING REMARKS

In this paper, we have proposed an innovative scheme to realize high-fidelity and long-distance transfer of an entangled state along a Y-shaped topologically nontrivial qubit chain in the presence of periodic driving. Before the state is transferred, a maximal entangled state is prepared through an adiabatic process, in which a key step is to introduce a nontrivial rotation between zero and π modes (both being topological edge states of the qubit chain). In the ideal situation, our QST can perfectly transfer an entangled state from one branch to another branch. In a more realistic situation, where disorder effects are introduced, the transfer fidelity is found to be robust against random noise, due to the inherent robustness of encoding qubits built from Floquet zero and π edge modes. Furthermore, one important property of our QST scheme is that the gap between the involved zero and π modes and the bulk states in the quasienergy spectrum does not scale down to zero as the size of the qubit chain increases. Thus, our scheme enables us to transfer the entangled qubits over long distance without the loss of topological protection or adiabaticity. Inspired by our QST scheme, we have also improved the QST protocol proposed in Ref. [26]. Indeed, one simple modification over the original protocol greatly enhances its robustness against disorder and also makes it possible to realize long-distance QST, but for single-qubit states only.

The potential applications of our QST protocol should lie in solid-state-based quantum information processing and quantum computation, where entangled qubits need to be transferred in certain solid-state devices over a not necessarily short distance. Given that topological edge modes, especially those of periodically driven systems, are already found to have great potential in implementing quantum computation protocols [21–23], it is stimulating to see by now that Floquet topological edge modes can further facilitate entangled state transfer along solid-state-based qubit chains.

ACKNOWLEDGMENTS

R.W.B. is supported by the Australian Research Council Centre of Excellence for Engineered Quantum Systems (EQUS, CE170100009). J.G. acknowledges funding support by the Singapore NRF Grant No. NRF-NRFI2017-04 (WBS No. R-144-000-378-281) and by the Singapore Ministry of Education Academic Research Fund Tier-3 (Grant No. MOE2017-T3-1-001 and WBS No. R-144-000-425-592).

APPENDIX A: ANALYTICAL CALCULATION OF ν_0 AND ν_π

We calculate the topological invariants ν_0 and ν_π of our system [see Eq. (4)]. As we discuss in the main text, ν_0 can be expressed in terms of $b(k)$ in the F matrix, which is explicitly given by

$$b(k) = e^{ik} \sin\left(\frac{j_2}{2}\right) \cos\left(\frac{J_1}{2}\right) + \cos\left(\frac{j_2}{2}\right) \sin\left(\frac{J_1}{2}\right). \quad (\text{A1})$$

Therefore,

$$\nu_0 = \frac{1}{2\pi i} \int_{-\pi}^{\pi} dk b^{-1} \frac{d}{dk} b \quad (\text{A2})$$

$$= \frac{1}{2\pi} \int_{-\pi}^{\pi} dk \frac{1}{1 + \frac{\tan J_1/2}{\tan j_2/2} e^{-ik}}. \quad (\text{A3})$$

It can be shown that for any real number A ,

$$\frac{1}{2\pi} \int_{-\pi}^{\pi} dk \frac{1}{1 + Ae^{-ik}} = \begin{cases} 1, & |A| < 1 \\ 0, & |A| > 1. \end{cases} \quad (\text{A4})$$

Since $\tan x$ is monotonically increasing in the range $x \in (0, \pi/2)$, the number of edge states with zero quasienergy (zero modes) is

$$\nu_0 = \begin{cases} 1, & j_2 > J_1 \\ 0, & j_2 < J_1. \end{cases} \quad (\text{A5})$$

The topological invariant ν_π can be calculated in a similar manner:

$$d(k) = \cos\left(\frac{j_2}{2}\right) \cos\left(\frac{J_1}{2}\right) - e^{-ik} \sin\left(\frac{j_2}{2}\right) \sin\left(\frac{J_1}{2}\right). \quad (\text{A6})$$

Therefore,

$$\nu_\pi = \frac{1}{2\pi i} \int_{-\pi}^{\pi} dk d^{-1} \frac{d}{dk} d \quad (\text{A7})$$

$$= \frac{1}{2\pi} \int_{-\pi}^{\pi} dk \frac{1}{1 - e^{ik} \cot(J_1/2) \cot(j_2/2)}. \quad (\text{A8})$$

As we discussed above, $\nu_\pi = 1$ if $|\cot(J_1/2) \cot(j_2/2)| < 1$. The inequality can be further simplified by using the trigonometry identity:

$$\cot(J_1/2) \cot(j_2/2) = \frac{\cos\left(\frac{J_1-j_2}{2}\right) + \cos\left(\frac{J_1+j_2}{2}\right)}{\cos\left(\frac{J_1-j_2}{2}\right) - \cos\left(\frac{J_1+j_2}{2}\right)}. \quad (\text{A9})$$

As $\cos\left(\frac{J_1-j_2}{2}\right) > 0$ when $0 < J_1, j_2 < \pi$, we only require $j_2 + J_1 > \pi$ to have $|\cot(J_1/2) \cot(j_2/2)| < 1$. Hence, the number of edge states with π/T quasienergy (π modes) is

$$\nu_\pi = \begin{cases} 1, & j_2 + J_1 > \pi \\ 0, & j_2 + J_1 < \pi. \end{cases} \quad (\text{A10})$$

APPENDIX B: DERIVATION OF $|0\rangle^{(L)}$ AND $|\pi\rangle^{(L)}$ DURING THE QST PROTOCOL

In this Appendix, we present the derivation of the zero and π modes at any stroboscopic time during the transfer protocol in Sec. IV.

1. Phase I

The Floquet operator U of our system can be written as a product of two exponentials,

$$U = \exp(-iH_2) \times \exp(-iH_1), \quad (\text{B1})$$

where the period T is now set to be 2 for brevity. To simplify our notation, we focus on the relevant terms in H_1 and H_2

which have support on the transferred zero and π modes. In the x th step, H_1 and H_2 read

$$H_1 = i\frac{\pi}{2}(\sigma_{A,2x-1}^{(L)\dagger}\sigma_{B,2x-1}^{(L)} + \sigma_{A,2x}^{(L)}\sigma_{B,2x}^{(L)} + \sigma_{A,2x+1}^{(L)\dagger}\sigma_{B,2x+1}^{(L)} + \text{H.c.}), \quad (\text{B2})$$

$$H_2 = i\pi(\sigma_{B,2x-1}^{(L)\dagger}\sigma_{A,2x}^{(L)} + \sin\phi_x\sigma_{A,2x-1}^{(L)\dagger}\sigma_{B,2x}^{(L)} + \cos\phi_x\sigma_{B,2x}^{(L)\dagger}\sigma_{A,2x+1}^{(L)} + \text{H.c.}), \quad (\text{B3})$$

where ϕ_x is adiabatically increased at every period from zero to $\pi/2$. It can be verified that

$$|0\rangle^{(L)} = \frac{1}{\sqrt{2}}[\cos\phi_x(|eg\rangle_{2x-1}^{(L)} - |ge\rangle_{2x-1}^{(L)}) + \sin\phi_x(|eg\rangle_{2x+1}^{(L)} - |ge\rangle_{2x+1}^{(L)})], \quad (\text{B4})$$

$$|\pi\rangle^{(L)} = \frac{1}{\sqrt{2}}[\cos\phi_x(|eg\rangle_{2x-1}^{(L)} + |ge\rangle_{2x-1}^{(L)}) + \sin\phi_x(|eg\rangle_{2x+1}^{(L)} + |ge\rangle_{2x+1}^{(L)})]. \quad (\text{B5})$$

Note that

$$\exp(-iH_1)|eg\rangle_{2x\pm 1}^{(L)} = |eg\rangle_{2x\pm 1}^{(L)}, \quad (\text{B6})$$

$$\exp(-iH_1)|ge\rangle_{2x\pm 1}^{(L)} = \pm|ge\rangle_{2x\pm 1}^{(L)}, \quad (\text{B7})$$

$$\exp(-iH_2)|ge\rangle_{2x\pm 1}^{(L)} = |ge\rangle_{2x\pm 1}^{(L)}, \quad (\text{B8})$$

$$\exp(-iH_2)|eg\rangle_{2x\pm 1}^{(L)} = \mp\cos 2\phi_x|eg\rangle_{2x\pm 1}^{(L)} + \sin 2\phi_x|eg\rangle_{2x\mp 1}^{(L)}. \quad (\text{B9})$$

By using Eqs. (B6) to (B9), one can directly verify that $U|0\rangle = |0\rangle$ and $U|\pi\rangle = -|\pi\rangle$.

2. Phase II

In a similar fashion, we can write H_1 and H_2 in the x th step as

$$H_1 = i\frac{\pi}{2}\sum_{m=1}^{x-1}(\sigma_{A,m-1}^{(R)\dagger}\sigma_{B,m-1}^{(R)} + \text{H.c.}) + i\frac{\pi}{2}\sum_{m'=1}^{N_M}(\sigma_{A,m'}^{(M)\dagger}\sigma_{B,m'}^{(M)} + \text{H.c.}), \quad (\text{B10})$$

$$H_2 = i\pi\sin\phi_x\sigma_{A,x-1}^{(R)\dagger}\sigma_{B,x}^{(R)} + i\pi\left(\sum_{m=1}^{x-1}\sigma_{A,m-1}^{(R)\dagger}\sigma_{B,m}^{(R)} + \sum_{m'=1}^{N_M}\sigma_{A,m'-1}^{(R)\dagger}\sigma_{B,m'}^{(R)}\right) + \text{H.c.}, \quad (\text{B11})$$

where $\sigma_{A,0}^{(R)\dagger} = \sigma_{A,N_L}^{(L)\dagger}$, $\sigma_{B,0}^{(M)\dagger} = \sigma_{B,0}^{(R)\dagger} = \sigma_{B,N_L}^{(L)\dagger}$, and ϕ_x is adiabatically increased at every period from zero to $\pi/2$. From the equations

$$\exp(-iH_1)|eg\rangle_{x(-1)}^{(R)} = |eg\rangle_{x(-1)}^{(R)}, \quad (\text{B12})$$

$$\exp(-iH_1)|ge\rangle_{x(-1)}^{(R)} = -|ge\rangle_{x(-1)}^{(R)}, \quad (\text{B13})$$

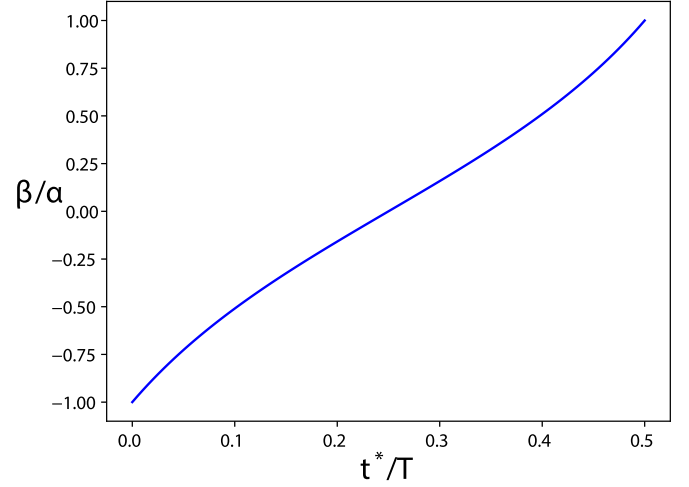


FIG. 10. The coefficient α as a function of t^* in the first half period of the time evolution.

$$\exp(-iH_2)|eg\rangle_{x-1}^{(R)} = \cos(\pi\sin\phi_x)|eg\rangle_{x-1}^{(R)} + \sin(\pi\sin\phi_x)|eg\rangle_x^{(R)}, \quad (\text{B14})$$

$$\exp(-iH_2)|ge\rangle_{x-1}^{(R)} = -|ge\rangle_{x-1}^{(R)}, \quad (\text{B15})$$

$$\exp(-iH_2)|eg\rangle_x^{(R)} = |eg\rangle_x^{(R)}, \quad (\text{B16})$$

$$\exp(-iH_2)|ge\rangle_x^{(R)} = -\sin(\pi\sin\phi_x)|eg\rangle_{x-1}^{(R)} + \cos(\pi\sin\phi_x)|ge\rangle_x^{(R)}, \quad (\text{B17})$$

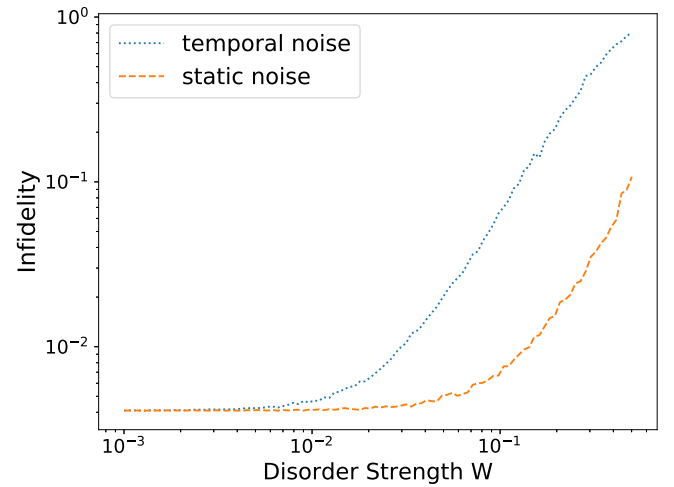


FIG. 11. Infidelity of the protocol under temporal noise as compared with that under static noise. The system parameters are $N_L = 22$, $N_R = 18$, and $N_M = 8$, with each step in the protocol taking 70 driving periods to complete. The protocol needs 14 steps in total to complete the QST. Results are obtained after averaging over 100 noise histories.

it can be verified that

$$|0\rangle^{(L)} = \frac{1}{\sqrt{2}} \left[\cos\left(\frac{\pi}{2} \sin \phi_x\right) (|eg\rangle_{x-1}^{(R)} - |ge\rangle_{x-1}^{(R)}) + \sin\left(\frac{\pi}{2} \sin \phi_x\right) (-|eg\rangle_x^{(R)} + |ge\rangle_x^{(R)}) \right], \quad (\text{B18})$$

$$|\pi\rangle^{(L)} = \frac{1}{\sqrt{2}} \left[\cos\left(\frac{\pi}{2} \sin \phi_x\right) (|eg\rangle_{x-1}^{(R)} + |ge\rangle_{x-1}^{(R)}) + \sin\left(\frac{\pi}{2} \sin \phi_x\right) (|eg\rangle_x^{(R)} + |ge\rangle_x^{(R)}) \right]. \quad (\text{B19})$$

APPENDIX C: DYNAMICAL STATE PREPARATION

This Appendix gives more details about the state preparation by using the dynamical phase within a driving period.

As described in the main text, a more generic state can be obtained by dynamically evolving the state. Suppose the initially prepared state is $|0\rangle = |eg\rangle_1 - |ge\rangle_1$; after the time evolution at specific time t^* , the state becomes $\alpha(t^*)|eg\rangle_1 + \beta(t^*)|ge\rangle_1$, where the numerical value of β/α is plotted in Fig. 10 for $0 \leq t^* \leq T/2$.

APPENDIX D: THE QST PROTOCOL UNDER TEMPORAL NOISES

This Appendix shows the numerical results of the infidelity of the QST protocol under temporal noises (see Fig. 11). Although the protocol is more vulnerable under temporal noises, it still shows robustness at small disorder strength. The temporal noise is introduced in a way that noise in different driving periods is independent, which is identical to the imperfect periodicity situation.

-
- [1] J. I. Cirac, P. Zoller, H. J. Kimble, and H. Mabuchi, *Phys. Rev. Lett.* **78**, 3221 (1997).
- [2] A. S. Parkins and H. J. Kimble, *J. Opt. B: Quantum Semiclass.* **1**, 496 (1999).
- [3] A. Gratsea, G. M. Nikolopoulos, and P. Lambropoulos, *Phys. Rev. A* **98**, 012304 (2018).
- [4] S. Bose, *Phys. Rev. Lett.* **91**, 207901 (2003).
- [5] M. Christandl, N. Datta, A. Ekert, and A. J. Landahl, *Phys. Rev. Lett.* **92**, 187902 (2004).
- [6] Z. Song and C. P. Sun, *Low Temp. Phys.* **31**, 686 (2005).
- [7] S. Bose, *Contemp. Phys.* **48**, 13 (2007).
- [8] V. Balachandran and J. Gong, *Phys. Rev. A* **77**, 012303 (2008).
- [9] N. Y. Yao, L. Jiang, A. V. Gorshkov, Z. X. Gong, A. Zhai, L. M. Duan, and M. D. Lukin, *Phys. Rev. Lett.* **106**, 040505 (2011).
- [10] X. Li, Y. Ma, J. Han, T. Chen, Y. Xu, W. Cai, H. Wang, Y. P. Song, Z.-Y. Xue, Z. Q. Yin, and L. Sun, *Phys. Rev. Appl.* **10**, 054009 (2018).
- [11] X. Z. Zhang, L. Jin, and Z. Song, *Phys. Rev. A* **85**, 012106 (2012).
- [12] A. Y. Kitaev, *Phys. Usp.* **44**, 131 (2001).
- [13] C. L. Kane and E. J. Mele, *Phys. Rev. Lett.* **95**, 146802 (2005).
- [14] M. Z. Hasan and C. L. Kane, *Rev. Mod. Phys.* **82**, 3045 (2010).
- [15] J. E. Moore, *Nature (London)* **464**, 194 (2010).
- [16] D. A. Ivanov, *Phys. Rev. Lett.* **86**, 268 (2001).
- [17] A. Kitaev, *Ann. Phys.* **321**, 2 (2006).
- [18] C. Nayak, S. H. Simon, A. Stern, M. Freedman, and S. Das Sarma, *Rev. Mod. Phys.* **80**, 1083 (2008).
- [19] N. Cooper, *Adv. Phys.* **57**, 539 (2008).
- [20] V. Lahtinen and J. K. Pachos, *SciPost Phys.* **3**, 021 (2017).
- [21] R. W. Bomantara and J. Gong, *Phys. Rev. Lett.* **120**, 230405 (2018).
- [22] R. W. Bomantara and J. Gong, *Phys. Rev. B* **98**, 165421 (2018).
- [23] R. W. Bomantara and J. Gong, *Phys. Rev. B* **101**, 085401 (2020).
- [24] N. Y. Yao, C. R. Laumann, A. V. Gorshkov, H. Weimer, L. Jiang, J. I. Cirac, P. Zoller, and M. D. Lukin, *Nat. Commun.* **4**, 1585 (2013).
- [25] C. Dłaska, B. Vermersch, and P. Zoller, *Quantum Sci. Technol.* **2**, 015001 (2017).
- [26] F. Mei, G. Chen, L. Tian, S.-L. Zhu, and S. Jia, *Phys. Rev. A* **98**, 012331 (2018).
- [27] S. Longhi, *Phys. Rev. B* **99**, 155150 (2019).
- [28] J. K. Asbóth and H. Obuse, *Phys. Rev. B* **88**, 121406(R) (2013).
- [29] J. K. Asbóth, B. Tarasinski, P. Delplace, *Phys. Rev. B* **90**, 125143 (2014).
- [30] D. Y. H. Ho and J. Gong, *Phys. Rev. B* **90**, 195419 (2014).
- [31] R. W. Bomantara, G. N. Raghava, L. W. Zhou, and J. Gong, *Phys. Rev. E* **93**, 022209 (2016).
- [32] R. W. Bomantara and J. Gong, *Phys. Rev. B* **94**, 235447 (2016).
- [33] H.-Q. Wang, M. N. Chen, R. W. Bomantara, J. Gong, and D. Y. Xing, *Phys. Rev. B* **95**, 075136 (2017).
- [34] L. Zhou and J. Gong, *Phys. Rev. A* **97**, 063603 (2018).
- [35] L. Zhou and J. Gong, *Phys. Rev. B* **98**, 205417 (2018).
- [36] L. Zhou and J. Gong, *Phys. Rev. B* **97**, 245430 (2018).
- [37] M. S. Rudner, N. H. Lindner, E. Berg, and M. Levin, *Phys. Rev. X* **3**, 031005 (2013).
- [38] Q. Cheng, Y. Pan, H.-Q. Wang, C. Zhang, D. Yu, A. Gover, H. Zhang, T. Li, L. Zhou, and S. Zhu, *Phys. Rev. Lett.* **122**, 173901 (2019).
- [39] M. Verbin, O. Zilberberg, Y. E. Kraus, Y. Lahini, and Y. Silberberg, *Phys. Rev. Lett.* **110**, 076403 (2013).
- [40] L.-Y. Zheng, V. Achilleos, O. Richoux, G. Theocharis, and V. Pagneux, *Phys. Rev. Appl.* **12**, 034014 (2019).
- [41] Y. Chen, C. Neill, P. Roushan, N. Leung, M. Fang, R. Barends, J. Kelly, B. Campbell, Z. Chen, B. Chiaro, A. Dunsworth, E. Jeffrey, A. Megrant, J. Y. Mutus, P. J. J. O'Malley, C. M. Quintana, D. Sank, A. Vainsencher, J. Wenner, T. C. White, M. R. Geller, A. N. Cleland, and J. M. Martinis, *Phys. Rev. Lett.* **113**, 220502 (2014).
- [42] R. Barends, J. Kelly, A. Megrant, D. Sank, E. Jeffrey, Y. Chen, Y. Yin, B. Chiaro, J. Mutus, C. Neill, P. O'Malley, P. Roushan, J. Wenner, T. C. White, A. N. Cleland, and J. M. Martinis, *Phys. Rev. Lett.* **111**, 080502 (2013).
- [43] M. R. Geller, E. Donate, Y. Chen, M. T. Fang, N. Leung, C. Neill, P. Roushan, and J. M. Martinis, *Phys. Rev. A* **92**, 012320 (2015).
- [44] J. Kelly, R. Barends, A. G. Fowler, A. Megrant, E. Jeffrey, T. C. White, D. Sank, J. Y. Mutus, B. Campbell, Y. Chen, Z. Chen, B. Chiaro, A. Dunsworth, I.-C. Hoi, C. Neill, P. J. J. O'Malley,

- C. Quintana, P. Roushan, A. Vainsencher, J. Wenner, A. N. Cleland, and J. M. Martinis, *Nature (London)* **519**, 66 (2015).
- [45] R. Barends, L. Lamata, J. Kelly, L. García-Álvarez, A. G. Fowler, A. Megrant, E. Jeffrey, T. C. White, D. Sank, J. Y. Mutus, B. Campbell, Y. Chen, Z. Chen, B. Chiaro, A. Dunsworth, I.-C. Hoi, C. Neill, P. J. J. O'Malley, C. Quintana, P. Roushan, A. Vainsencher, J. Wenner, E. Solano, and J. M. Martinis, *Nat. Commun.* **6**, 7654 (2015).
- [46] J. H. Shirley, *Phys. Rev.* **138**, B979 (1965).
- [47] H. Sambe, *Phys. Rev. A* **7**, 2203 (1973).
- [48] One may notice that the chiral symmetry operator defined earlier, i.e., $\Gamma = \tau_z$, maps $|0\rangle^L$ to $|\pi\rangle^L$ and vice versa, in contrast to the expected behavior that zero and π modes are eigenstates of the chiral symmetry operator. This is because $\Gamma = \tau_z$ only represents the chiral symmetry operator in the symmetric time frame, which amounts to taking $t_0 = T/4$ in Eq. (3). In the time frame where the QST protocol is executed, where $t_0 = 0$ in Eq. (3), the chiral symmetry operator is obtained through a unitary transformation $\Gamma' = \exp(iH_1T/4)\tau_z \exp(-iH_1T/4) = \tau_x$, where $|0\rangle^L$ and $|\pi\rangle^L$ can indeed be identified as its eigenstates.
- [49] M.-T. Rieder, L. M. Sieberer, M. H. Fischer, and I. C. Fulga, *Phys. Rev. Lett.* **120**, 216801 (2017).
- [50] S. Choi, J. Choi, R. Landig, G. Kucsko, H. Zhou, J. Isoya, F. Jelezko, S. Onoda, H. Sumiya, V. Khemani, C. von Keyserlingk, N. Y. Yao, E. Demler, and M. D. Lukin, *Nature (London)* **543**, 221 (2017).
- [51] J. W. McIver, B. Schulte, F.-U. Stein, T. Matsuyama, G. Jotzu, G. Meier, and A. Cavalleri, *Nat. Phys.* **16**, 38 (2020).
- [52] D. A. Abanin, W. De Roeck, and F. Huveneers, *Ann. Phys. (Amsterdam)* **372**, 1 (2016).
- [53] P. Ponte, A. Chandran, Z. Papić, and D. A. Abanin, *Ann. Phys. (Amsterdam)* **353**, 196 (2015).
- [54] P. Ponte, Z. Papić, F. Huveneers, and D. A. Abanin, *Phys. Rev. Lett.* **114**, 140401 (2015).
- [55] A. Lazarides, A. Das, and R. Moessner, *Phys. Rev. Lett.* **115**, 030402 (2015).
- [56] D. V. Else, B. Bauer, and C. Nayak, *Phys. Rev. X* **7**, 011026 (2017).
- [57] D. V. Else, B. Bauer, and C. Nayak, *Phys. Rev. Lett.* **117**, 090402 (2016).